JOURNAL OF THERMOPHYSICS AND HEAT TRANSFER
Vol. 13, No. 4, October–December 1999

Transient Studies of G-Induced Capillary Flow

M. K. Reagan*
Air Force Institute of Technology, Wright–Patterson Air Force Base, Ohio 45433-7765
and
W. J. Bowman†
Brigham Young University, Provo, Utah 84602

A transient, one-dimensional numerical code is developed to model liquid motion in a square groove. Transient body forces up to 0.51 m/s^2 are investigated. Axial variation in liquid level, shear stress and heat transfer between the groove wall and the liquid, evaporation, and body forces are accounted for in the model. Dryout and rewet of the groove are allowed; the front location is determined using conservation of mass. An experiment is presented that measures the depth of liquid in the groove and the dryout and rewet front locations during a transient. Within the uncertainty of the measurements, the code predicts the correct liquid distribution and front locations.

Nomenclature

A = liquid cross-sectional flow area
A^* = nondimensional area, $A/w\delta$
$\tilde{A}$ = groove area over which shear acts
A_{in} = groove area across which heat energy flows
c_p = liquid specific heat
D_h = hydraulic diameter based on A
d_{ep} = distance between the last wet node and the extinction point
E = total energy per unit mass
$\bar{E}$ = spatial derivative matrix
f = friction coefficient
g = gravitational constant, 9.81 m/s^2
h = average liquid depth, A/w
h_{in} = heat-transfer coefficient between the groove wall and the liquid
h_l = liquid height parameter, $1 - h_p/\delta$
h_p = meniscus depth parameter
L_∞ = axial groove length
m = liquid mass
$\dot{m}_e$ = evaporative mass flow rate
Nu = Nusselt number
P = average liquid pressure
P_∞ = ambient pressure
Q_{cond} = energy transfer rate caused by axial conduction in the liquid
Q_{in} = energy transfer rate between the groove wall and the liquid
Q_{out} = energy transfer rate between the liquid and the environment
R = meniscus radius of curvature
$\bar{S}$ = source matrix
T = bulk liquid temperature
T_g = groove wall temperature
t = time
t_∞ = experimental run time
t^* = nondimensional time, t/t_∞
$\bar{U}$ = temporal derivative matrix
V = liquid velocity
V_e = evaporative velocity
w = groove width
x = axial location from the center of rotation
x^* = nondimensional axial location, x/L_∞
γ = angle describing meniscus variation
δ = groove depth
λ = latent heat of vaporization
ρ = density
σ = surface tension coefficient
τ = shear stress between groove wall and liquid
ψ = groove tilt angle
Ω = groove rotation rate
$\forall$ = volume

Introduction

HEAT pipes and capillary-driven evaporators have been proposed as a means of thermal management in the aerospace industry. Uses include electronics cooling, hypersonic aircraft engine inlet and leading-edge cooling, and thermal management of space-based platforms.[1–4]

The environment of the aerospace vehicle is a dynamic one where transient body forces primarily affect the movement of the working fluid within the capillary structure, or wick, of these devices. Traditionally, these devices have been used in environments where body forces were either steady or negligible. Acceptance of these devices as the primary means of cooling in the aerospace environment will depend, then, on a thorough understanding of their operation under the expected transient G loading.

Literature on the effect of transient body forces on the performance of capillary-driven heat-transfer devices is limited. A transient heat pipe modeling workshop held at the NASA John H. Glenn Research Center at Lewis Field in September of 1990 concluded the most important part of the transient heat pipe problem was modeling the liquid flow in the wick. Recommendations suggested that more physical experiments geared toward understanding the liquid flow under transient conditions be conducted, especially liquid flow under transient G loading.

Yerkes et al.[5] studied the performance of a flexible copper/water heat pipe subjected to transverse and axial accelerations between 1.1 and 9.8 G and 0.01 and 0.03 Hz. Results of the study indicated partial dryout of the wick at higher accelerations. A reduction in the applied accelerations was mentioned as the most effective method for rewetting the pipe. Theoretical analysis dealt only with the steady behavior of increased body forces on the pipe's performance; no attempt was made to model the liquid flow.

Hawthorne[6] studied the effect of transient body forces on the liquid flow in a single, heated capillary groove. Dryout and rewet

Presented as Paper 94-2029 at the AIAA/ASME 6th Joint Thermophysics and Heat Transfer Conference, Colorado Springs, CO, 20–23 June 1994; received 14 September 1998; accepted for publication 29 March 1999.

*Assistant Professor of Aerospace Engineering, Department of Aeronautics and Astronautics. Member AIAA.
†Associate Professor of Mechanical Engineering, Mechanical Engineering Department. Senior Member AIAA.

in the groove caused by the transient body force was observed. In addition to some general observations on the shape and behavior of the f ront, the extent of dryout was found to depend on the magnitude and duration of the body force transient. No analytical model of the liquid flow was provided.

Several investigators have numerically modeled the transient liquid flow in a heated capillary structure.[7–9] One limitation of these models is that the body force is only treated in a steady-state manner. Another limitation is that none of them realistically models the shape or behavior of the liquid front. Visual observations of Hawthorne confirmed liquid recession along the groove up to the front location. None of the preceding models allows for recession; in fact, each models the wick as either full or empty, with the interface between the full and empty regions described as planar and perpendicular to the liquid flow direction.

Experimental work has shown that transient body forces can cause dryout and rewet of a capillary structure. However, the capability to realistically model unsteady capillary flow subject to transient body forces is inadequate. A new numerical model is therefore warranted.

Theory

Several assumptions are made concerning the derivation of the governing equations.[10] The capillary structure is a square groove with constant width w and depth δ. One end of the groove can be tilted relative to the other end. This provides the transient body force. No flooding of the groove is allowed (i.e., the depth of liquid in the groove is always less than or equal to δ), and the pressure above the liquid in the groove is assumed constant and equal to ambient pressure P_∞.

The working liquid is ethanol and is assumed to be incompressible with density, $\rho = 785$ kg/m^3. Laminar flow within the groove is assumed at all times, and kinetic and potential energy changes are considered negligible with respect to the internal energy of the liquid. Free convection and radiation losses to the environment are also considered negligible with respect to the energy lost by evaporation.

Consider the control volume shown in Fig. 1. This control volume encompasses the liquid only and not the groove structure. The liquid flow is from left to right, and the meniscus level is assumed to vary linearly through the control volume.

The equation of conservation of mass for this control volume, noting that $\rho\,\mathrm{d}x$ is constant, yields

$$\frac{\partial A}{\partial t} + \frac{\partial (AV)}{\partial x} + \frac{\dot{m}_e}{\rho\,\mathrm{d}x} = 0 \tag{1}$$

Figure 2 shows the same control volume with the appropriate forces (solid arrows) and momentum terms (dashed arrows). The groove with the liquid is tilted at an angle ψ around a center of rotation relative to horizontal level, and this angle is a function of time, which provides the transient body force $\rho A g \sin\psi\,\mathrm{d}x$, where g is the gravitational constant.

Momentum changes within the liquid, evaporative momentum flux ($\dot{m}_e V_e \sin\gamma$), shear force between the groove wall and the liquid ($\tau\tilde{A}$), and capillary forces $(p_\infty - \sigma/R)w\tan\gamma\,\mathrm{d}x$ are also modeled, where γ is the axial variation of the liquid depth, V_e is the velocity with which the evaporative mass flow leaves the control volume, and σ is the ethanol surface tension coefficient.

The meniscus radius of curvature R is a function of the liquid cross-sectional flow area and therefore can vary with axial location x. The $(\rho A\Omega^2 x)\,\mathrm{d}x$ term accounts for the noninertial reference frame of the governing equations, where Ω is the groove rotation rate.

Newton's second law for this control volume then is given by Eq. (2):

$$\frac{\partial (AV)}{\partial t} + \frac{\partial}{\mathrm{d}x}\left(AV^2 + \frac{PA}{\rho}\right) = \frac{\dot{m}_e V_e \sin\gamma}{\rho\,\mathrm{d}x} - Ag\sin\psi$$
$$- \frac{\tau\tilde{A}}{\rho\,\mathrm{d}x} - \frac{1}{\rho}\left(p_\infty - \frac{\sigma}{R}\right)w\tan\gamma + A\Omega^2 r \tag{2}$$

The average liquid pressure P at any axial location is assumed to be the ambient pressure minus the capillary pressure because of the curved interface, plus the pressure head caused by the depth of the liquid in the groove. The average depth of liquid in the groove h is approximated by $h = A/w$, and the average pressure head can be shown to be $0.5\rho g h\cos\psi$. The average liquid pressure then is a function of the groove tilt angle ψ, the cross-sectional flow area A, and the meniscus radius of curvature R.

The radius of curvature is a function of the liquid cross-sectional flow area and is assumed to behave as shown in Fig. 3. When the groove is entirely full of liquid, there is no meniscus, and the radius of curvature is infinite. As liquid evaporates or is moved by

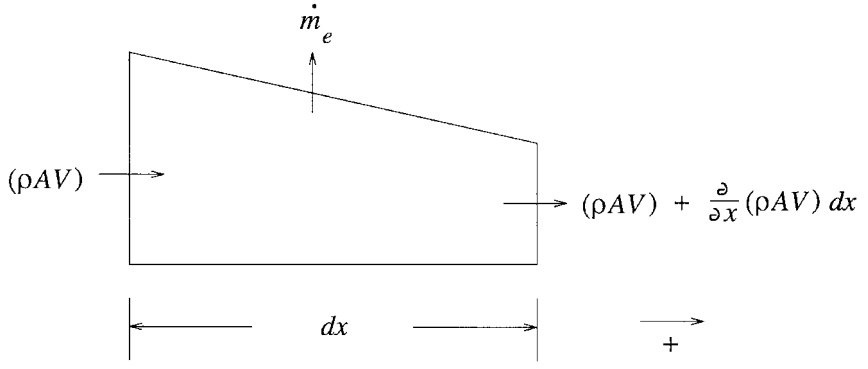

Fig. 1 Continuity control volume.

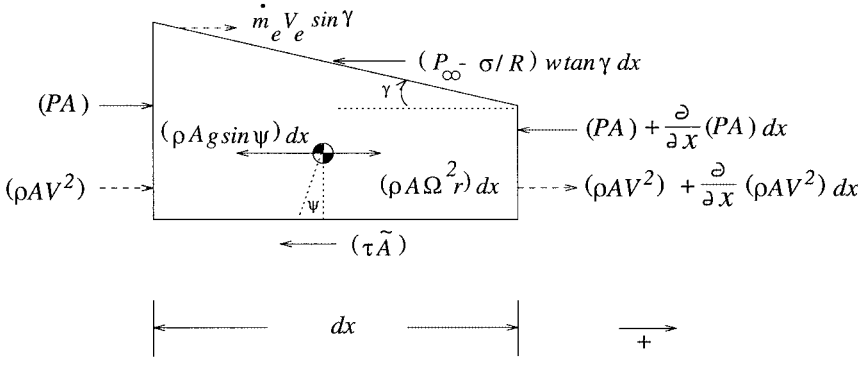

Fig. 2 Momentum control volume.

bulk motion, the meniscus recedes into the groove, and R decreases from infinity until a hemispherical shape is formed. The radius of curvature at this condition is $R = w/2$. This hemispherical shape remains fixed until the tangent to the meniscus is coincident with the bottom of the groove. As more liquid is removed by bulk motion or evaporation, the meniscus recedes further into the corners of the groove, and the radius of curvature continues to decrease. This decrease in radius is only allowed to continue until the resulting liquid pressure is zero.

The shear stress between the groove wall and liquid τ is calculated using

$$\tau = f\rho V^2/2 \tag{3}$$

The friction coefficient f in Eq. (3) is determined using rectangular tube flow data from Shah[11] and modified for channel flow according to Chi.[12] The remaining quantities in Eq. (2) (evaporative mass flow, groove tilt angle, and angular rotation rate) are experimentally measured quantities and will be discussed in the Experiment section.

The energy equation for this system is derived using the control volume in Fig. 4. The total energy is approximated by the internal energy $E \approx c_p T$, where c_p is the liquid specific heat and T is the bulk liquid temperature.

The energy influx Q_{in} is modeled using $Q_{\text{in}} = h_{\text{in}} A_{\text{in}} (T_g - T)$. This coefficient was calculated using

$$h_{\text{in}} = Nuk/D_h \tag{4}$$

where k is the liquid thermal conductivity. Nu was determined using convection correlations for constant surface heat flux, laminar tube flow,[13] and corrected for channel flow similar to the method used for the friction coefficient.[12]

Q_{out} is the rate of heat energy exiting the control volume and was determined using $Q_{\text{out}} = \dot{m}_e \lambda$, where λ is the latent heat of vaporization. Q_{cond} is the rate of energy conducted axially through the control volume and was calculated using Fourier's conduction law. The equation for conservation of energy for the control volume of Fig. 4, therefore, is

$$\frac{\partial}{\partial t}(AE) + \frac{\partial}{\partial x}\left[AV\left(E + \frac{P}{\rho}\right)\right] = \frac{(Q_{\text{in}} - Q_{\text{out}})}{\rho\, dx} - \frac{1}{\rho}\frac{\partial Q_{\text{cond}}}{\partial x} \tag{5}$$

Equations (1), (2), and (5) form the set of governing equations for the new model. The pressure-area and radius-area relationships already discussed provide closure for the system.

The temporal derivative terms are grouped into a 3×1 matrix $\bar{U}$, and the spatial derivative terms are grouped together into a 3×1 matrix $\bar{E}$. The remaining terms are combined into a source term $\bar{S}$, and the resulting system is written as

$$\bar{U}_t + \bar{E}_x = \bar{S} \tag{6}$$

where the subscripts t and x refer to the time and space derivatives, respectively. Equation (6) is nondimensionalized and integrated using a first-order-accurate, explicit Roe scheme.[14] Details of the solution methodology and code validation are found in Ref. 10. The sensitivity of the solution results to numerical grid was studied. The number of grid points was doubled until solution convergence was obtained. The excellent agreement between numerical and experimental results also supported the adequacy of the numerical grid used.

Boundary Conditions

The integration is performed on a one-dimensional grid. Node 1 lies on the left boundary; this node is also the center of rotation of the groove. As such, it always contains some liquid, and because of the physical boundary, the velocity is always zero. The grid extends to I nodes, some or all of which have liquid in them, depending on the dryout/rewet front location. Node nb refers to the last wet node and is only equal to node I if the groove is fully wet. The grid remains fixed to the groove structure and does not move with the liquid.

At time level n the total mass of liquid in the groove m_g is known. At time level $n+1$, assuming only evaporation, the total mass of liquid in the groove is

$$m_g^{n+1} = m_g^n - \sum_{i=2}^{\text{nb}} \dot{m}_e \Delta t \tag{7}$$

The mass in any control volume is found by using

$$m_i = 0.5\rho\Delta x(A_i + A_{i-1}) \tag{8}$$

Applying the principle of conservation of mass to the leftmost control volume yields the area of node 1 as

$$m_2^{n+1} = m_2^n - \Delta t\left(\dot{m}_2^n + \dot{m}_e^n\right) \Rightarrow A_1^{n+1} = \frac{2m_2^{n+1}}{\rho\, dx} - A_2^{n+1} \tag{9}$$

where $\dot{m}_2$ is the rate of mass leaving node 2 via the groove. The velocity at node 1 is zero because of the physical boundary, and the temperature is updated assuming an adiabatic end condition.

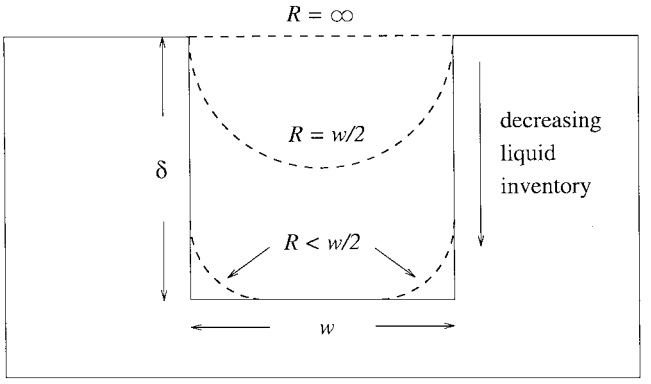

Fig. 3 Meniscus behavior in a square groove.

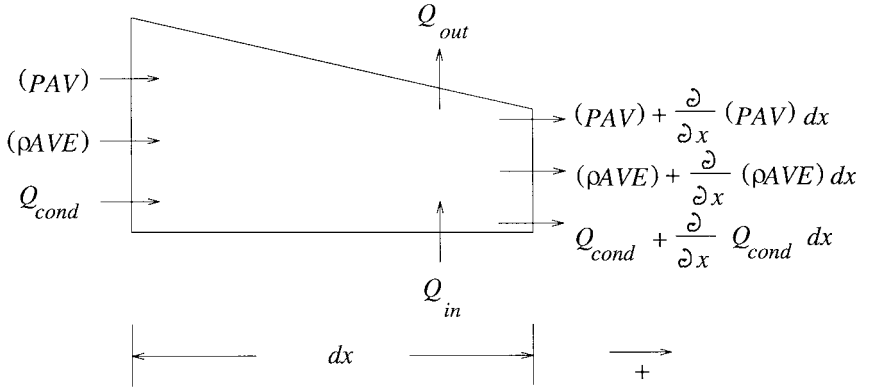

Fig. 4 Energy control volume.

The rightmost control volume in the groove m_r at time level $n+1$ is

$$m_r^{n+1} = m_g^{n+1} - m_{\text{int}}^{n+1} - m_2^{n+1} \tag{10}$$

where m_{int} is the mass in all interior nodes along the groove.

If the groove is not in a state of dryout, then m_r occupies node I and the area at node I is

$$A_I^{n+1} = \frac{2m_r^{n+1}}{\rho \Delta x} = -A_{I-1}^{n+1} \tag{11}$$

The velocity is identically zero, and the temperature is updated assuming an adiabatic end condition.

If, however, the groove is exhibiting dryout or rewet, then a front exists, and m_r occupies some specified volume extending beyond the last wet node. Linear interpolation was used to find the length of the wet region past the last wet node. Defining the location in the groove where the cross-sectional flow area is zero at the extinction point ep, then the distance between the last wet node (node nb) and the extinction point is

$$d_{\text{ep}} = \frac{2m_r^{n+1}}{\rho A_{\text{nb}}^{n+1}} \tag{12}$$

The boundary conditions at the extinction point are

$$A_{\text{ep}} = 0 \qquad \left|\frac{\partial A}{\partial x}\right|_{\text{ep}} = \frac{-\rho\left(A_{\text{nb}}^{n+1}\right)^2}{2m_r^{n+1}} \tag{13}$$

If d_{ep} is less than Δx, then m_r is not sufficient to extend the triangular profile to node nb + 1. In this case the area, velocity and temperature distributions of the liquid are completely defined, and no further calculations are required.

If, however, d_{ep} is greater than Δx, then m_r is sufficient to extend the profile to node nb + 1. In this case $A_{\text{nb}+1}^{n+1}$ is calculated using the area at node nb and the slope from Eq. (13). Applying conservation of mass on the control volume between the last wet nodes and the new last wet node (nb + 1) yields the velocity as

$$V_{\text{nb}+1}^{n+1} = \left[(AV)_{\text{nb}}^{n+1} - \left(\frac{\partial \forall}{\partial t}\right)_{\text{nb}+1} - \frac{\dot{m}_e}{\rho}\right] \Big/ A_{\text{nb}+1}^{n+1} \tag{14}$$

where $\forall$ is the volume. A first-order approximation to the volume derivative term is used, and the evaporation term is evaluated at the temperature of node nb at time $n+1$. The temperature is updated assuming no axial conduction.

After the area velocity and temperatures are updated, the mass in the new control volume is subtracted from m_r, and a new m_r is established. Node nb + 1 is renumbered as node nb, and a new d_{ep} value is calculated. The procedure just described is repeated until this new d_{ep} is less than Δx.

Experiment

The experimental portion of the work was divided into two tests. The first test measured the evaporation rate of ethanol as a function of temperature; the second test measured the liquid distribution of ethanol in the heated groove structure as a function of time. The second test provided the data necessary to validate the numerical model.

Evaporation Test

A cylindrical vessel with a 17.4-mm-diam circular opening was placed on a digital scale, and a thermocouple was placed within the vessel. The scale and thermocouple were connected to a data acquisition system that recorded the temperature and mass of the ethanol in the vessel as a function of time. A heater was placed between the vessel and the scale to maintain the ethanol at different temperatures between ambient and its boiling point.

A typical run was accomplished by heating the ethanol within the vessel to a steady-state temperature, which depended on the amount of input power to the heater. The acquisition system was activated, and the mass was recorded as a function of time. Because the temperature was held constant, the slope of the mass vs time data was expected to be linear. The slope provided the mass flow at the given temperature, and a least-squares analysis provided the error associated with the measurement.

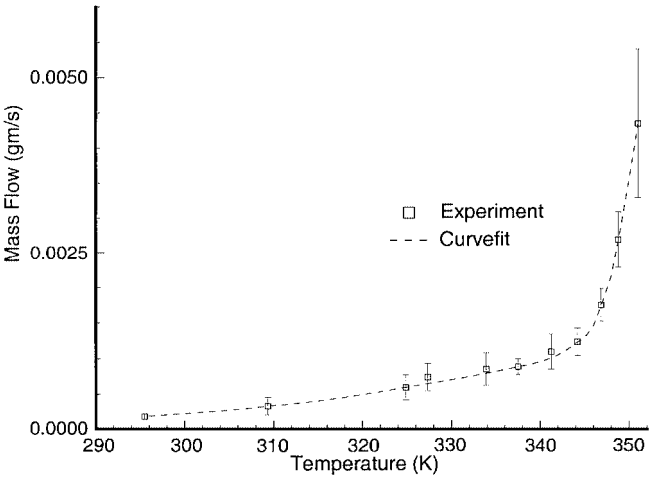

Fig. 5 Ethanol mass flow results.

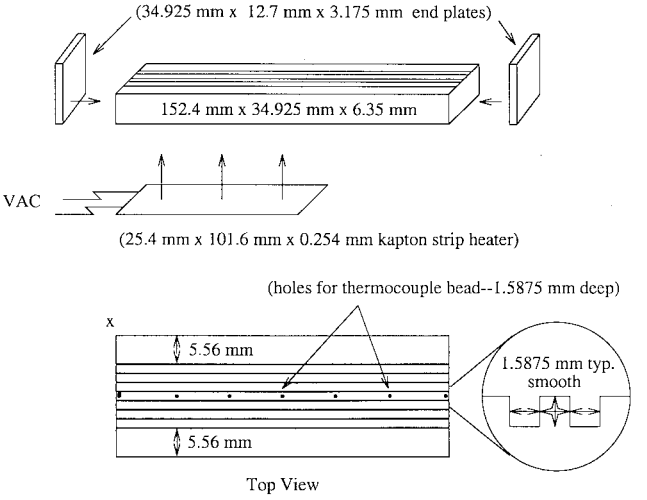

Fig. 6 Groove substructure.

This test was performed for several different heater power settings (corresponding to different ethanol temperatures), and the results are seen in Fig. 5. The squares depict the experimentally determined mass flow, the vertical lines are the associated uncertainty, and the dashed line is the curve fit through the data. Uncertainty in the temperature measurement was ± 0.5 K. This curve fit was input to the code as the required evaporation model.

Evaporation rate was assumed to only be a function of temperature and was found from the experiment just described. This method for estimating evaporation was selected over an evaporation correlation to eliminate one possible source of error. An evaporation correlation could have been used in the model; however, it may not have been as accurate as the correlation found for the specific experiment in question.

Groove Test

The groove substructure was made of stainless steel with dimensions shown in Fig. 6. Eight identical square grooves were milled into the top of the plate along its entire length. An endplate was welded onto each end to prevent liquid outflow. Seven equally spaced thermocouples were cemented into the peak between the two center grooves with a high conductivity cement. A strip heater was epoxied to the bottom of the groove.

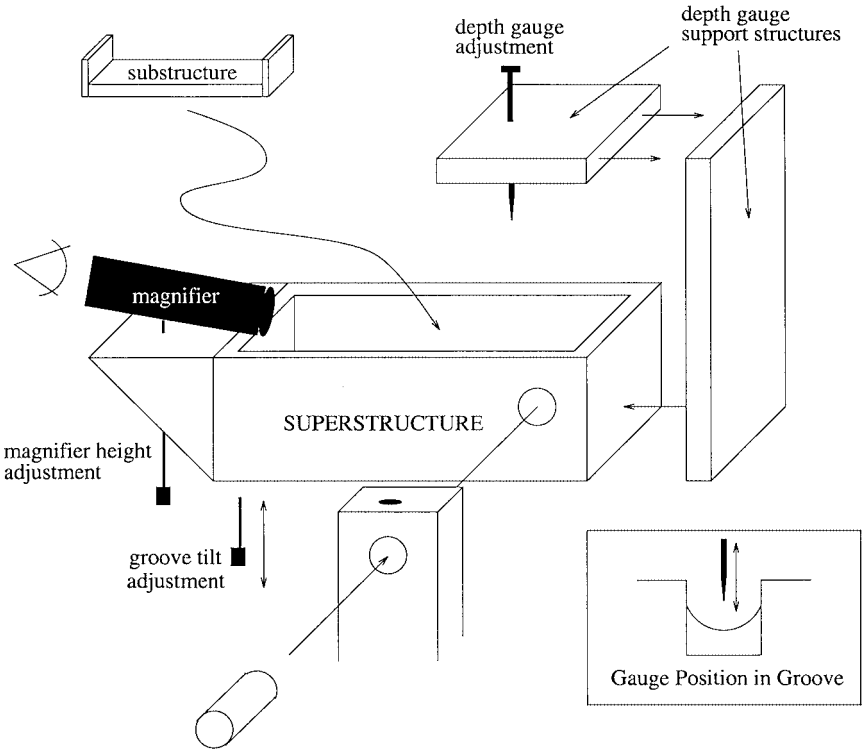

Fig. 7 Groove superstructure.

The substructure was placed into a cavity milled into a plexiglass superstructure with dimensions shown in Fig. 7. The groove was held in place with silicone cement, which helped to thermally insulate the groove. The superstructure was placed in a fork mount, which allowed it to rotate via a tilt adjustment control. A depth gauge was mounted and positioned on the superstructure so that the gauge could traverse into and out of the center of a groove as shown in the insert. The axial position of this gauge could be moved between test runs but was fixed for any particular run. A magnifier was also installed to monitor the depth gauge movement into the groove.

A typical data run for this test began by leveling the groove with an inclinometer and positioning the depth gauge 19.05 mm from the center of rotation. Nondimensionalizing by the groove length L_∞ this was an axial position of $x^* = 0.125$. The grooves were flooded with ethanol, and evaporation was allowed to occur until the depth gauge could be lowered into the groove a distance of 0.79 mm and be in close proximity to the liquid meniscus. This depth was termed h_p. The magnifier was used to ensure that the gauge did not touch the liquid surface, and the uncertainty in this measurement was ± 0.08 mm. Nondimensionalizing by the total cross-sectional flow area, this gauge measurement resulted in a distribution of $A^* = 0.607$. This established a baseline condition from which all further tests were begun.

From this condition the groove was rotated through the angular schedule shown in Fig. 8. Interval 1 tilted the groove at a rate of $+0.0175$ rad/min for the first 3 min. Between 3 and 4 min (interval 2), the groove was maintained at 0.0524 rad. Between 4 and 6 min (interval 3), the groove was lowered at a rate of -0.0262 rad/min so that it was at the initial level conditions by the end of the test.

This schedule was chosen to provide a test of two different onset rates of the transient body force. Noting that the body force is approximately $g \sin \psi$, then interval 1 resulted in a maximum body force of 0.51 m/s^2 at a frequency of 2.8 mHz, whereas interval 3 resulted in the same magnitude body force but at a frequency of 4.2 mHz. The reason that the maximum body force was so low was because of the flooding restriction discussed earlier. Because the grooves could not be flooded, the maximum angle of the groove structure was approximately 0.05 rad or 8.0 mm.

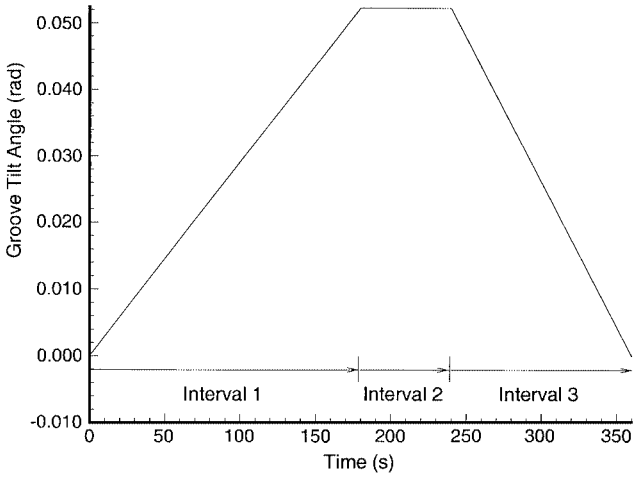

Fig. 8 Groove tilt schedule.

Throughout the groove rotation depth-gauge measurements were made at approximate 1-min intervals, and when a front appeared, its location was noted and recorded. For this test a front was defined to exist when the level of liquid in the groove was sufficient so that the tangent to the meniscus was coincident with the bottom of the groove, as shown in Fig. 9. With this definition the liquid that remained in the groove was concentrated in the corners, and the nondimensional cross-sectional flow area was $A^* = 0.107$.

The groove test was performed with the power to the heater turned off to establish the baseline and then with the power on to simulate the heated capillary structure. The thermocouple readings for the power on tests are seen in Fig. 10 and are accurate to ± 0.5 K. Time measurements are accurate to ± 0.01 s.

A choice needed to be made between using the heater power into the plate or using the plate temperature as a boundary condition. If heater power had been used, the temperature of the plate would need to be estimated numerically. To reduce error, the temperature boundary condition was measured directly and used as the boundary condition.

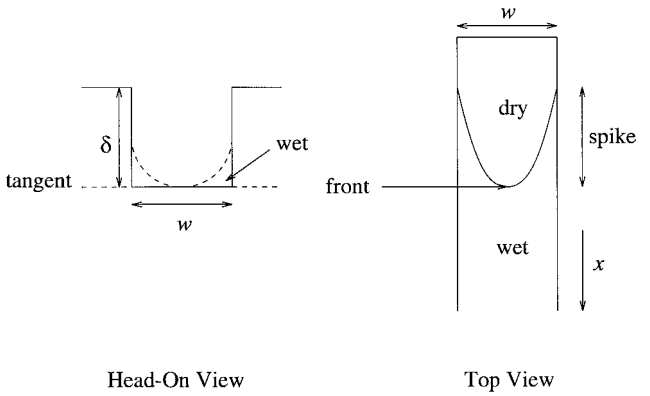

Fig. 9 Front location definition.

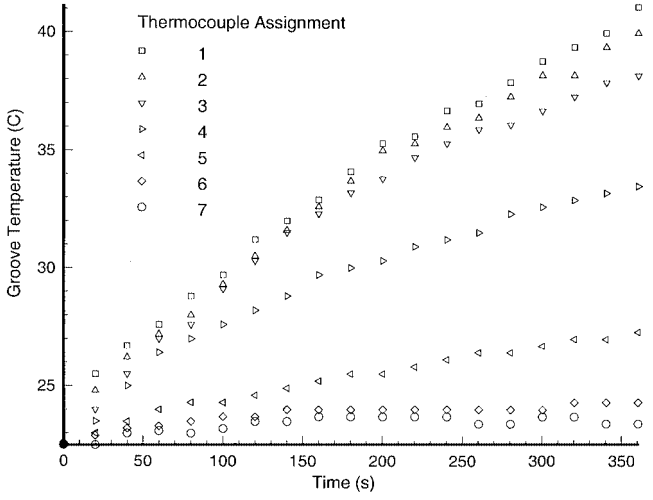

Fig. 10 Groove heating schedule.

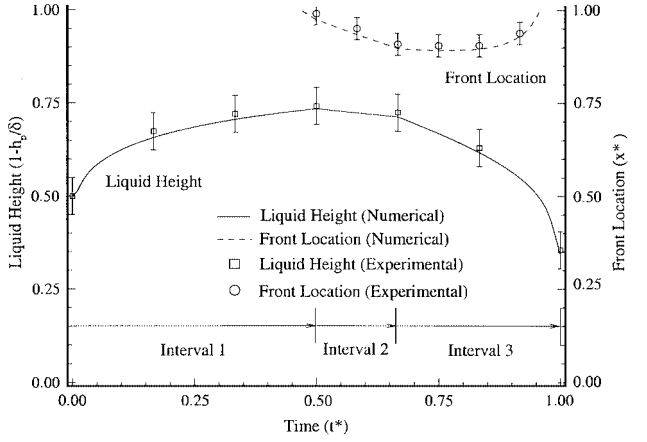

Fig. 11 Power-off test results ($x^* = 0.125$).

Results and Discussion

The results of the power-off test are shown in Fig. 11. Four sets of data are on this figure: the lines corresponding to the numerical results and the symbols corresponding to the experimental results. The horizontal axis is nondimensional time t^*, where $t^* = t/t_\infty$. The t_∞ for this experiment was 360 s. The left vertical axis is nondimensional liquid height, defined as $h_l = 1 - h_p/\delta$, and the right vertical axis is nondimensional front location.

The solid line in Fig. 11 represents the liquid height in the groove predicted by the numerics. At the beginning of the experiment, the liquid height is $h_l = 0.50$, corresponding to the initial condition just described. As the groove is rotated up (interval 1), liquid flows toward the gauge position and the distance the gauge can be lowered into the groove before touching the liquid surface is reduced. This corresponds to a rise in the liquid height.

During interval 2, the liquid height decreases. Whereas liquid momentum and gravity are still causing bulk liquid motion toward $x^* = 0$, evaporation appears to offset these effects and causes an overall decrease in the liquid height. During interval 3 as the groove is leveled, the liquid height decreases more rapidly than the rate observed during interval 1 because of the increased frequency of the body force during this interval; i.e., 50% higher than during interval 1.

At the end of the data run, the liquid height is approximately $h_l = 0.34$. This is noticeably lower than the initial height of $h_l = 0.50$, indicative of evaporation occurring.

The squares in Fig. 11 represent the average of the measured liquid heights from two experimental runs. The vertical lines on the liquid height curve represent the uncertainty associated with the depth-gauge measurement. The numerics capture the correct trends and properly model the liquid motion.

The bias in the experimental data could be caused by the method used to measure the liquid height. Because the depth gauge is always lowered from above the liquid to a position just above the liquid surface, and because the gauge never comes in contact with the surface, there is most likely a tendency to prematurely stop the gauge motion. This would lead to experimental values greater than those predicted by theory, as seen in Fig. 11.

The dashed line in Fig. 11 represents the dryout front position as predicted from the numerics. From the figure the beginning of dryout is predicted toward the end of interval 1 and continues through interval 2 and into interval 3. The numerics show that as the rotation back to level is begun at $t^* = 0.67$ the liquid responds almost immediately and the rewet is completed at $t^* = 0.96$. The maximum distance the front travels axially into the groove structure, defined as the extent of dryout, is approximately $x^* = 0.88$ and occurs at $t^* = 0.76$.

The circles in the figure represent the average of the measured front locations from the same two experimental runs. The vertical lines on the front location curve represent the uncertainty in this measurement, ±5 mm. The numerics capture the correct trends and properly model the behavior of the liquid front within the uncertainty of the measurements.

Figure 12 shows the results of the power-on test. The axes and their definitions are identical to those discussed for the power-off case. From Fig. 12 one can see that the initial time of dryout occurs earlier, full rewet occurs later, and the extent of dryout is more pronounced than for the power-off test. Definitions of the experimental quantities and their associated uncertainties are identical to those for Fig. 11. Again, the numerics capture the correct trends and properly model the behavior of the liquid front within the uncertainty of the measurements.

To get a full appreciation for the differences between the power-off and power-on cases, the numerical results for each case are plotted against one another and are seen in Fig. 13. Comparing the liquid

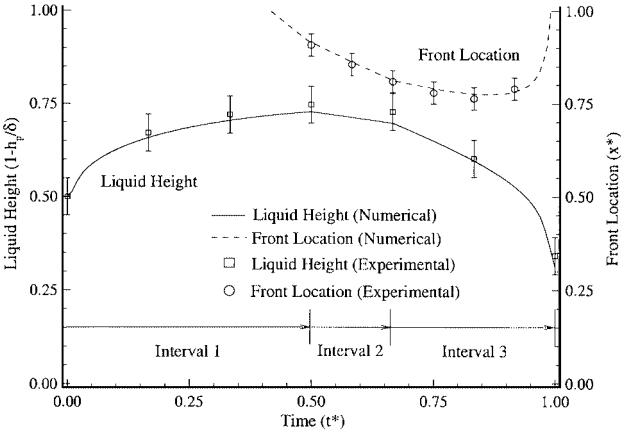

Fig. 12 Power-on test results ($x^* = 0.125$).

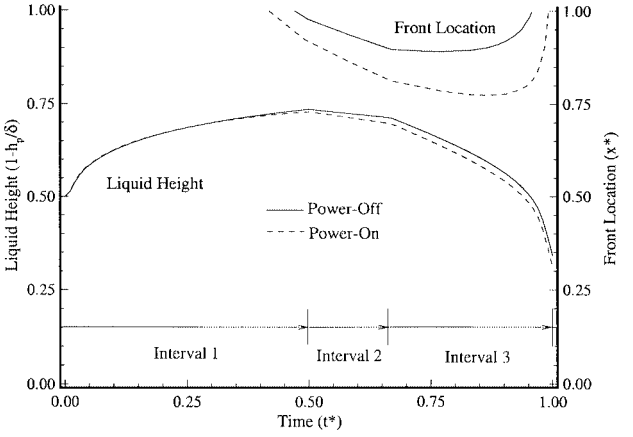

Fig. 13 Comparison between power-off and power-on test ($x^* = 0.125$).

height curves, the power-off data lie a maximum of 3% above the power-on data with the predominant deviations occurring in intervals 2 and 3. The reason is caused by the increased evaporation in the power-on test as a result of the increased liquid temperatures caused by the external heating. The curves do not deviate until interval 2 because of the finite time required to heat the liquid in the groove.

Comparing the front location curves shows the primary effects of external heating. The first difference is the time at which initial dryout occurs: earlier in interval 1 for the power-on test. The second difference is the rate at which dryout progresses, greater for the power-on test as evidenced by the steeper slope of the front location curve. The third difference is the extent of dryout, which is 11% greater for the power-on test.

The most interesting difference between the two front location curves is the behavior of the front during interval 3. In the power-off test the front begins to recover and rewet the groove almost immediately ($t^* = 0.67$), whereas the front in the power-on test continues its dryout behavior until approximately $t^* = 0.90$. At this point the front reverses direction and begins to rewet the groove.

This behavior is caused by the dryout that occurs in the power-on test because of external heating. External heating causes the groove to heat up faster in the dried-out area than in the area that is still wet with ethanol. When the groove is lowered and the ethanol begins to rewet the hot groove surface, the amount of liquid that evaporates is greater than that being supplied by the bulk liquid motion because of the transient body force generated by the lowering of the groove. However, once sufficient momentum is generated by the body force, the front reverses direction, and rewet begins. Full rewet occurs at approximately $t^* = 0.99$.

Conclusions

Transient body forces can influence the liquid motion in a heated capillary structure. The influence of these body forces can cause a dryout of the groove structure and by proper application can also effect a rewet of dried-out regions. The motion of the liquid subject to transient body forces, along with the capability to predict dryout and rewet, can be accurately modeled numerically.

Acknowledgments

This research was sponsored by the U.S. Air Force Aero Propulsion and Power Directorate of Wright Laboratory. The comments and suggestions of Jerry Beam were greatly appreciated.

References

[1]Peterson, G. P. , "Heat Pipes in the Thermal Control of Electronic Components," *Proceedings of the 3rd International Heat Pipe Symposium*, Tsukuba City, Japan, Sept. 1988.

[2]Colwell, G. T., "Cooling Hypersonic Vehicle Structures," *Proceedings of the 7th International Heat Pipe Conference*, Minsk, USSR, 1990.

[3]Yerkes, K. L., and Hager, B. G., "Transient Response of Heat Pipes for Actuator Thermal Management," *SAE Aerospace Atlantic Conference*, Society of Automotive Engineers, TP Series 92-1024, 1992.

[4]Müller, R., "Analysis of the Liquid Distribution in Capillary Grooves of a SpacePlane Evaporation Cooler," *Proceedings of the 8th International Heat Pipe Conference*, Beijing, Sept. 1992.

[5]Yerkes, K. L., Chang, W. S., and Beam, J. E., "Heat Pipe Performance with Transient Heat Flux and Body Force Effects," *Proceedings of the 8th International Heat Pipe Conference*, 1992.

[6]Hawthorne, Capt. L. S., "Rewet Performance of a Rectangular Grooved Heat Pipe Wick After Gravitationally Induced Dryout," M.S. Thesis, Department of Aeronautics and Astronautics, Air Force Inst. of Technology, Wright-Patterson AFB, OH, Dec. 1993.

[7]Holderness, J. H., "Operation of a Heat Pipe Beyond the Capillary Limit," Ph.D. Dissertation, Dept. of Mechanical Engineering, Univ. of Michigan, Ann Arbor, MI, 1973.

[8]Beam, J. E., "Transient Heat Pipe Analysis," AIAA Paper 85-0936, June 1985.

[9]Ambrose, J. H., Chow, L., and Beam, J., "A Detailed Model for Transient Liquid Flow in Heat Pipe Wicks," AIAA Paper 90-0062, Jan. 1990.

[10]Reagan, M. K., "Transient Body Force Effects on the Dryout and Rewet of a Heated Capillary Structure," Ph.D. Dissertation, Department of Aeronautics and Astronautics, Air Force Inst. of Technology, Wright-Patterson AFB, OH, April 1994.

[11]Shah, R. K., and London, A. L., *Laminar Flow Forced Convection in Ducts*, Academic, New York, 1978, p. 190.

[12]Chi, S. W., *Heat Pipe Theory and Practice*, McGraw-Hill, New York, 1976, pp. 40, 41.

[13]Kays, W. M., and Crawford, M. E., *Convective Heat and Mass Transfer*, 2nd ed., McGraw-Hill, New York, 1987, p. 103.

[14]Roe, P. L., "Approximate Riemann Solvers, Parameter Vectors, and Difference Schemes," *Journal of Computational Physics*, Vol. 43, No. 2, 1981, pp. 357–372.